

Disorder-induced delocalization and reentrance in a Chern-Hopf insulator

Soumya Bera,¹ Ivan Dutta,^{2,3} Roderich Moessner,⁴ and Kush Saha^{2,3}

¹*Department of Physics, Indian Institute of Technology Bombay, Mumbai 400076, India*

²*National Institute of Science Education and Research, Jatni, 752050, India*

³*Homi Bhabha National Institute, Training School Complex, Anushakti Nagar, Mumbai 400094, India*

⁴*Max-Planck Institute for the Physics of Complex System, Dresden, Germany*

(Dated: August 8, 2024)

The Chern-Hopf insulator is an unconventional three-dimensional topological insulator with a bulk gap and gapless boundary states without protection from global discrete symmetries. This study investigates its fate in the presence of disorder. We find it stable up to moderate disorder by analyzing the surface states and the zero energy bulk density of states using large-scale numerical simulation and the self-consistent Born approximation. The disordered Chern-Hopf insulator shows reentrant behavior: the disorder initially enhances the topological phase before driving it across an insulator-diffusive metal transition. We examine the associated critical exponents via finite-size scaling of the bulk density of states, participation entropy, and two-terminal conductance. We estimate the correlation length exponent $\nu \simeq 1.0(1)$, consistent with the *clean* two-dimensional Chern universality and distinct from the integer quantum Hall exponent.

I. INTRODUCTION

It is generally understood that for disorder-driven quantum phase transitions, i.e., Anderson transitions, the symmetry of the underlying Hamiltonian and its spatial dimensions solely determine the universality class and the corresponding critical exponents [1]. Whether or not introducing band topology will preserve the universality class of the transition depends on the underlying symmetries of the disordered potential and has been a subject of intense research in the last couple of decades, e.g., see Refs. [2–8]. While non-spatial symmetries of standard topological insulators are expected to protect the surface states [9, 10], the disorder can disrupt them [11–13]. Interestingly, these states remain stable under weak to moderate disorder as long as symmetry and the bulk gap are preserved [14]. Adding disorder can even enhance the topological phase by effectively renormalizing system parameters from an initially trivial parameter regime [15–26]. Eventually, increasing disorder drives the system into a diffusive metallic regime and induces standard Anderson localization, transitioning the system from a diffusive metal to an insulating phase [27–29].

The situation becomes intriguing with non-conventional topological insulators outside the standard 10-fold classification scheme [30]. The stability of these insulators, which are protected by generic crystalline symmetries [31–37] – such as the axion insulators [38–40] and higher-order topological insulators [41–49] – in the presence of the disorder have received considerable attention in recent years. For instance, disorder can induce a bulk quantum phase transition in an inversion-symmetric three-dimensional (3D) axion insulator, characterized by a localization exponent $\nu \simeq 1.42(10)$ [39]. In contrast, the surface of such an insulator exhibits a phase transition between the axion insulating phase and the Anderson insulating phase driven by magnetic disorder, with the critical point

showing 2D quantum Hall criticality characterized by a critical exponent $\nu \simeq 2.6(2)$ [40].

Another class of unconventional 3D topological insulators¹, which lack topological protection from conventional discrete symmetries, is the Hopf insulators [51–61] and are characterized by a non-zero Hopf index [51, 62–66]. They are described by a minimal two-band model, $\mathcal{H}(\mathbf{k}) = \mathbf{d}(\mathbf{k}) \cdot \boldsymbol{\sigma}$, where $\boldsymbol{\sigma} = \{\sigma_x, \sigma_y, \sigma_z\}$ represents a set of Pauli matrices, and $\mathbf{d} = \{d_x, d_y, d_z\}$ encodes a bulk gap that prevents a continuous deformation of the Hamiltonian into a trivial \mathbf{k} -independent Hamiltonian. From the homotopy perspective, the momentum \mathbf{k} belongs to the three torus T^3 , representing the Brillouin zone. The unit vector $\mathbf{d}(\mathbf{k})/|\mathbf{d}(\mathbf{k})|$ identifies a point in the two-sphere S^2 ; thus, the Hamiltonian can be considered a map from T^3 to S^2 . The three 2D planes xy , yz , and xz of T^3 can have non-zero Chern number C_α , where $\alpha \in (x, y, z)$. For $C_\alpha = 0$, the Hopf insulators are constructed by an intermediate map: a point on T^3 to a point in three-sphere S^3 , then to a point in S^2 via a Hopf map. This non-trivial mapping results in an integer-valued Hopf invariant. Conversely, when $C_\alpha \neq 0$, the invariant takes values in the finite group $Z_{2 \cdot \text{gcd}(C_x, C_y, C_z)}$, where gcd denotes the greatest common divisor. These insulators are termed Chern-Hopf insulators (CHI). We focus on a scenario where any two-dimensional slice of the 3D Brillouin zone carries a finite Chern number [67] and features non-trivial gapless boundary states, such as a nodal ring (see Fig. 1). We aim to understand the effect of disorder on the CHI phase and the corresponding boundary states, which lack protection from non-crystalline symmetry.

We observe that the boundary states remain stable un-

¹ We note that Hopf insulators are sometimes considered a subclass of axion insulators [50]. However, the axion insulators mentioned earlier, protected by inversion symmetry, differ from Hopf insulators, characterized by a combination of time-reversal and reflection symmetries.

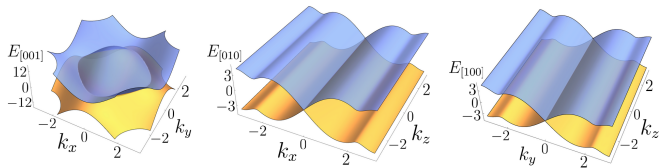


FIG. 1. Surface states dispersion along the (001), (010), and (100) directions: a Dirac nodal ring in the (001) plane, and a Dirac line at zero energy in both (010) and (100) planes, differing from typical Dirac nodes on conventional topological insulator surfaces. We use periodic boundary conditions in the directions perpendicular to the surface under consideration. The parameters in Eq. (2) are taken to be $t_2 = -2$, $h = -4$, and $t = 5$.

der weak to moderate disorder. However, as the disorder increases, the CHI phase transitions into a diffusive metal phase, qualitatively characterized by the closing of the bulk gap and the disappearance of the boundary states. Additionally, numerical simulations show that disorder enhances the topological phase, a result we confirm using the self-consistent Born approximation (SCBA). We further investigate the critical properties of this transition through a scaling analysis of several observables, including the density of states $\rho(E)$, participation entropy \mathcal{S}_1 , and two-terminal conductance g . Remarkably, we observe that the correlation length exponent closely matches the universality class of the two-dimensional clean Chern insulator with $\nu \simeq 1.0(1)$. Finally, we discuss the potential material realization of the Chern-Hopf model.

II. MODEL

A generic 3D tight-binding Hamiltonian, defined on a cubic lattice in which each lattice site contains two orbital states $|A\rangle$, $|B\rangle$, with nearest-neighbor (NN) and next-nearest neighbor hopping (NNN) can be written as [68]

$$H_{3D} = \sum_{\mathbf{r}, \mu, \nu} |\mathbf{r} + \mathbf{e}_\mu\rangle \gamma^{\mu\nu} \langle \mathbf{r} + \mathbf{e}_\nu|, \quad (1)$$

where \mathbf{r} denotes lattice site, $\mathbf{e}_0 = (0, 0, 0)$ is the null vector and $\mathbf{e}_{\mu(\nu)}$ is the vector encoding the six-fold coordination via $\mathbf{e}_{1, \dots, 6} = \{x, y, z, xy, xz, yz\}$, respectively. The coordinates, for example, x , xy represent vectors $(1, 0, 0)$, $(1, 0, 1)$, respectively, $\gamma^{\mu\nu}$ are hopping matrices involving sublattices. With this, the minimal CHI model can be constructed with the following matrices:

$$\begin{aligned} \gamma^{0,0} &= h \sigma_z; \gamma^{1,0} = t \sigma_z; \gamma^{2,0} = t \sigma_z; \\ \gamma^{5,0} &= -\frac{t_2}{2}(\sigma_x + i\sigma_y); \gamma^{1,3} = \frac{t_2}{2}(\sigma_x - i\sigma_y); \\ \gamma^{6,0} &= \frac{t_2}{2}(\sigma_y - i\sigma_x); \gamma^{3,2} = \frac{t_2}{2}(i\sigma_x - \sigma_y), \end{aligned} \quad (2)$$

where σ_i 's are the Pauli matrices and h, t, t_2 are the model parameters. This is equivalent to constructing a

2D Chern model in the $x - y$ plane and extending it in the z -direction to construct the 3D model. The corresponding momentum space Hamiltonian takes the following form, $H(\mathbf{k}) = d(\mathbf{k}) \cdot \sigma$, where

$$\begin{aligned} d_x(\mathbf{k}) &= 2t_2(\sin k_x \sin k_z + \cos k_z \sin k_y), \\ d_y(\mathbf{k}) &= 2t_2(-\sin k_y \sin k_z + \cos k_z \sin k_x), \\ d_z(\mathbf{k}) &= h + 2t(\cos k_x + \cos k_y). \end{aligned} \quad (3)$$

We note that a minimum tight-binding model of a Hopf insulator without any non-zero Chern number requires NNN hopping [68].

The CHI Hamiltonian in Eq. 1 exhibits two topological invariants: Chern number ($C_z = 1$) in the xy plane and a 3D Hopf invariant ($h_f = 1$). For $-4t < h < 0$, we obtain a gapped insulating phase with $C_z = 1$ and for $0 < h < 4t$, we obtain $C_z = -1$. In both cases, the Hopf invariants are found to have integer values with $|h_f| = 1$. The bulk gap closes at $h = |4t|$, and for $h > |4t|$, we obtain a trivial insulating phase with both C_z and h_f to be zero.

To find the surface states for different planes as shown in Fig. (1), we numerically solve the tight-binding Hamiltonian in Eq. (1) with open boundaries along z , y and x , respectively. In certain cases, the effective Hamiltonian for the surface states can be obtained numerically, as shown in Appendix C. The surface states of (001) turn out to be a nodal ring, while the surface states for (010) and (100) are line Dirac nodes.

To address the effect of disorder, we add onsite local magnetic disorder² to Eq. (1), in the form $H_{\text{dis}} = \sum_{\mathbf{r}} |\mathbf{r}\rangle_{\alpha} U_{\alpha\alpha} \langle \mathbf{r}|$, where $U_{\alpha\alpha} = U(\mathbf{r})\sigma_z$. We consider the disorder potential $U(\mathbf{r})$ distributed uniformly over the interval $[-W, W]$. In the continuum description, we take $\langle U(\mathbf{r}) \rangle = 0$ and, $\langle U(\mathbf{r})U(\mathbf{r}') \rangle = \frac{W^2}{3}\delta(\mathbf{r} - \mathbf{r}')$, where $\delta(\mathbf{r})$ is the Dirac delta function. In all numerical simulations we choose $t = 1.0$, and $t_2 = 1.0$ unless mentioned otherwise.

III. RESULTS AND DISCUSSION

Stability of the surface mode: Probing the stability of surface states against disorder provides insights into their topological protection, as discussed previously for topological insulators [14] and, more recently, for Weyl surface states [69]. We start discussing the evolution of the surface mode in the (001) direction of the Hopf insulator (1) in the presence of onsite disorder. The momentum-resolved boundary spectral function is de-

² The critical properties of the Hopf-insulator to diffusive metal transition are unaffected by local charge impurity disorder instead of magnetic disorder. The corresponding data is shown in App. A.

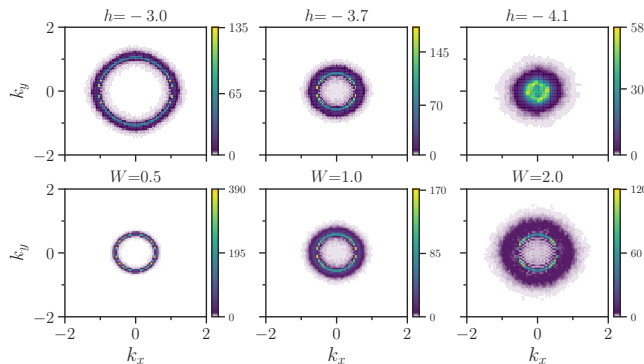


FIG. 2. Evolution of the surface state along the (001) direction as seen in momentum resolved surface spectral function, $\mathcal{A}(\mathbf{k}, E)$ (4) at $E = 0$ (color bar represents the value in arbitrary units). Top row: for different h -parameter as defined in Eq. (2). Bottom row: for different disorder strengths W . The delocalization transition is signified by the decrease in the radius of the nodal ring in the upper panel and by the decrease in the spectral weight of the surface mode in the lower panel. The system size is $\{L_x, L_y, L_z\} = \{128, 128, 64\}$.

fined as,

$$\mathcal{A}(\mathbf{k}, E) = \sum_{j=1}^{\mathcal{D}} \sum_{\alpha=1}^2 |\psi_j^s(k_x, k_y, \alpha)|^2 \delta(E - E_j), \quad (4)$$

where j, α denote the spatial index and the orbital degrees, respectively; $\psi_j^s(\vec{k}, \alpha)$ denotes the $E = 0$ momentum resolved surface wavefunction at the (001) boundary. We approximate the delta function in Eq. (4) with a box function by considering only four surface states close to zero energy, calculated using standard diagonalization techniques.

The upper panel of Figure 2 illustrates the spectral function across various h values with a fixed disorder of $W = 1.1$. The nodal ring at $E = 0$ broadens due to disorder, and its radius decreases as h nears the gap-closing threshold. Near the critical point, $h_c \simeq -4.1$, the ring structure ceases to exist, signaling a transition to a metallic state without the topological surface state.

In the lower panel of Fig. 2, the same surface mode is shown for a fixed value $h = -3.7$ with increasing disorder. The state survives at weak disorder; however, with spectral broadening, a typical response to the disorder, as also observed in 3D topological insulators [14]. As disorder increases beyond $W \gtrsim 1$, the ring expands progressively until it disappears, qualitatively coinciding with the closure of the bulk gap, as seen in Fig. 5. In App. B, the evolution of the topological surface state in the (100)-direction is shown, corroborating the similar physics observed in the (001) direction.

Density of states (DOS): The disorder averaged bulk DOS $\bar{\rho}(\varepsilon = 0)$ acts as an order parameter for the transition; here, overline denotes the averaging over different disorder configurations. The transition to diffusive metal is signaled by a finite density of state at $\varepsilon = 0$ as shown

in Fig. 5. The raw data calculated by diagonalizing the Eq. (1) is shown in Fig. 3(a) for different system sizes L across the transition driven by the field h . In the metallic phase, the normalized density of state $\bar{\rho}(0) = L^{-2} \bar{\rho}(0)$ is finite, while in the localized phase, it vanishes with increasing system size. Generically, the following scaling form is usually used to perform the finite size scaling analysis,

$$\bar{\rho}(0) = \sum_{j=0}^{N_R} a_j x^j + b L^{-y} + c b L^{-y} x, \quad (5)$$

where $x = (h - h_c)/h_c \cdot L^{1/\nu}$, the h_c is the critical field, and ν is the leading scaling exponent, and the N_R is the expansion order, which usually chosen to be $N_R = 2$, to reduce the number of fitting parameters a_j, b, c ³. We use least-square fitting to determine the coefficients a_j , and the critical parameters h_c, ν . The finite size collapse of $\rho(0)$ is shown in Fig. 3(d) with a critical exponent $\nu \simeq 1.1(1)$, and $h_c \simeq -4.116(4)$.

Participation entropy: Across the transition, we probe the nature of the state through the participation entropy [71], defined as

$$\mathcal{S}_1 = - \sum_{\mathbf{r}} \sum_{\alpha} |\psi_{\alpha}(\mathbf{r})|^2 \ln |\psi_{\alpha}(\mathbf{r})|^2,$$

where $\psi_{\alpha}(\mathbf{r})$ is the bulk wavefunction at $E = 0$ calculated using shift-invert diagonalization. In the insulating phase, \mathcal{S}_1 is constant for finite L , while in the metal phase $\mathcal{S}_1 = \ln \mathcal{D}$, where \mathcal{D} is the Hilbert space dimension. Figure 3(b) shows the renormalized $\bar{\mathcal{S}}_1 / \ln \mathcal{D}$, for different system sizes, across the transition. At the critical point, the participation entropy is finite, signaling a metallic point, while in the localized phase, increasing L makes it vanish trivially. The corresponding collapse, Fig. 3(e), of $\bar{\mathcal{S}}_1 / \ln \mathcal{D}$, obtained using the same scaling function (5) with $N_R = 2$ yields critical parameters consistent with DOS data.

Two terminal conductance: The disorder averaged two-terminal conductance \bar{g} along the z-direction of the sample with length L and width W is obtained from the Landauer formulation of transport, i.e., $g = (e^2/h) \text{Tr}(t^\dagger t)$, where t is the transmission matrix. We employ the quantum transport code `Kwant` [72]: two infinitely long cubic leads are attached in the z-direction. The lead is represented by the same Hamiltonian (1) as in the scattering region with $h = 0$.

Figure 3(c) shows $\ln \bar{g}$, which acts as an order parameter [73, 74] at the metal-insulator transition, for several combinations of L, W , and h . As it turns out, within this

³ In the scaling ansatz, we ignore the irrelevant scaling variables; the justification comes from the observation that in standard 3D disordered models, the irrelevant correction to scaling is small, i.e., y is large [70]. Nonetheless, we checked (data is not shown) and found that it does not change the reported critical exponent.

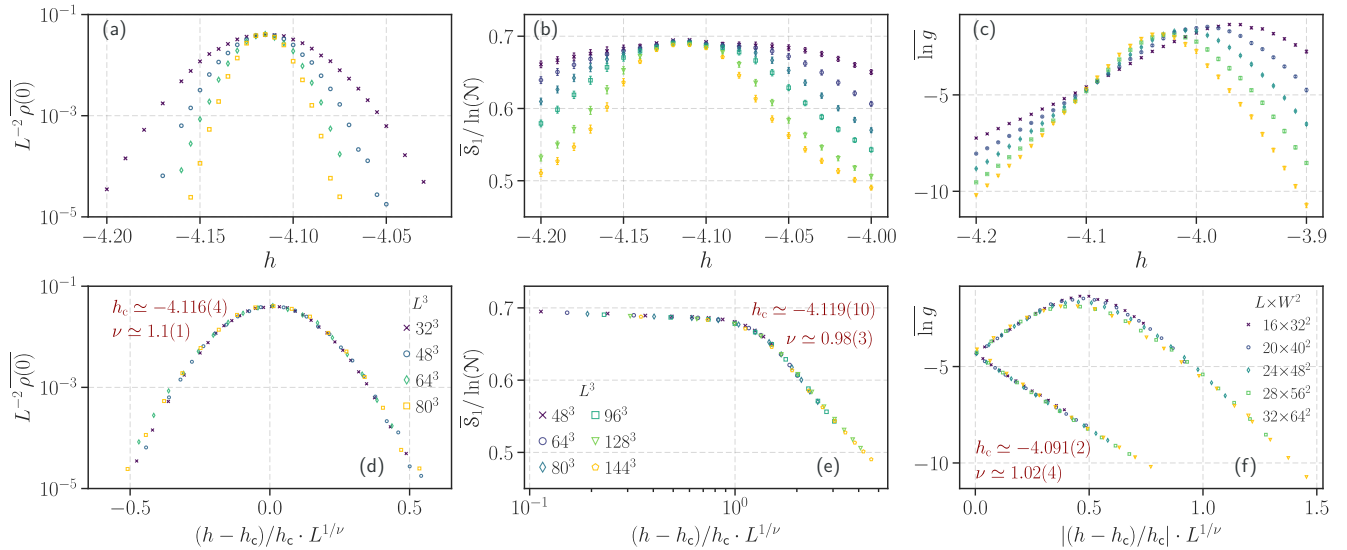


FIG. 3. (a) The zero energy DOS $\bar{\rho}(\varepsilon = 0)$ for cubes of linear length of $L = 32, 48, 64, 80$ across the transition driven by h . (b) Renormalized participation entropy $\bar{S}_1/\ln(\mathcal{D})$ across the same transition for different L . (c) Two terminal conductance $\ln(g)$ at $\varepsilon = 0$ for samples of length L along the transport direction, and W the width of the perpendicular direction (see panel (f)). (d-f) Corresponding scaling collapses with $h_c \simeq -4.11$, and $\nu \simeq 1.0$, consistent within the least-square fitting errors (mentioned in the plots) for all the observables.

setup, the conductance value is small $g \ll 1$ at the critical point, which is related to the choice of the parameter $h = 0$ in the lead. This, however, does not affect the scaling analysis. On the insulating side, $\ln g$ decreases as expected from $g \sim \exp(-L/\xi)$. In contrast, in the Hopf insulating side, there is an initial increase of $\ln g$, as the localization length $\xi \gtrsim L$, and with increasing L , the data crosses over to insulating behavior. Plotting as a function of scaling variable $(h - h_c)/h_c \cdot L^{1/\nu}$ in Fig. 3(e), the metallic branch is visible on the Hopf-side, and only when $L > \xi$, it shows the scaling of the insulating phase. The scaling exponent $\nu \simeq 1.02(4)$ is consistent with all the previous observables.

Dynamical scaling: We calculate the DOS using the standard Kernel polynomial method (KPM) [75]. Here, the DOS is expanded in terms of Chebyshev polynomials, $T_n(x)$, $\rho(\varepsilon) = \text{Tr} \delta(\varepsilon - H) \approx \mu_0 + 2 \sum_{n=1}^{N_m} g_n \mu_n T_n(\varepsilon)$. The trace, Tr , is stochastically estimated using $N_{\text{tr}} = 8$ random vectors in a 128^3 system. We compute Chebyshev moments, μ_n , and apply the Jackson kernel, g_n , to mitigate the Gibbs oscillations arising from a finite number of terms in the Chebyshev expansion N_m .

At finite energy, we assume the following scaling form of the density of states close to the transition approaching from the metallic side,

$$\rho(\varepsilon) \sim \delta^{(d-z)\nu} \mathcal{F}(|\varepsilon| \delta^{-z\nu}),$$

where $d = 3$, and z is the dynamical critical exponent, and $\delta = (W - W_c)/W_c$. \mathcal{F} is an unknown scaling function that depends on the energy ε , and we expand it up to the second order in the scaling variable. Figure 4 shows the rescaled $\rho(\varepsilon) \cdot \delta^{-(3-z)\nu}$ against the scal-

ing variable $\varepsilon \delta^{-z\nu}$ for several values of disorder W for fixed $h = -3.7$ as shown with a vertical dashed line in the Fig. 5, i.e., unlike previously, now approaching the transition from the metallic side with fixed h . The inset shows the raw DOS data for those disorder strengths. The single parameter scaling yields a dynamical exponent as $z \simeq 0.85(5)$. This could be contrasted with the following observation that near the quantum critical point, at small energies $\rho(\varepsilon) \sim \varepsilon^2$, suggesting $z \approx 1.0$ from the scaling analysis [76–79]. This can be attributed to the Dirac nature of the low-energy dispersion at the clean bulk gap closing point $h = -4t$. At the Γ point The dispersion can be derived from the continuum description $E(k_x, k_y) \simeq \pm [4t_2^2(k_x^2 + k_y^2)]^{1/2}$, which is independent of the k_z .

Phase diagram: Figure 5 shows the phase diagram of the CHI (1) in the presence of disorder close to a gap closing point, $h = -4.0$. Due to finite N_m , the $\rho(0)$ is always finite even in the insulating phase. Using $\rho(0) \lesssim 10^{-4}$ as an indicator of the vanishing density of states, we observe an increase of the Chern-Hopf phase with increasing W , indicated by the re-entrant phase boundary similar to the disordered topological phase in 2D [80, 81]. At higher disorder values the system enters the diffusive metal phase. One would expect the standard Anderson localization transition to occur at even higher disorder values, which we do not probe in this study.

Self-consistent Born Approximation (SCBA): In the presence of disorder, the Green's function of the electron obeys $G(\omega, \mathbf{k}) = (\omega - H(\mathbf{k}) - \Sigma)^{-1}$. Here, the self-energy of the electron can be evaluated within the self-consistent

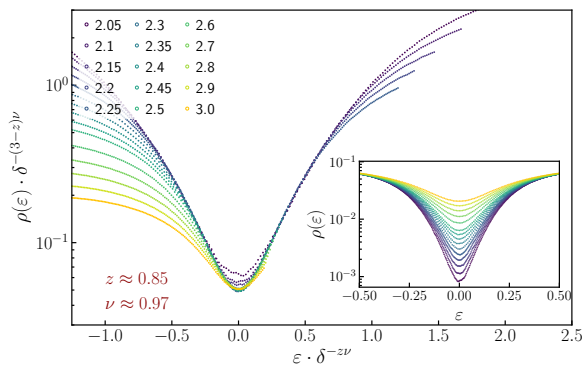


FIG. 4. Scaling collapse of the density of states at finite energy ε for $L = 128$ on the metallic side for different disorder values mentioned in the legend. Inset shows the raw $\rho(\varepsilon)$ before rescaling. At energies $\varepsilon \approx 0$, we observe the effects of the finite number of expansion moments, $N_m=8193$. We average over approximately 100 disorder configurations.

Born approximation (SCBA):

$$\Sigma(\omega) = \frac{W^2}{3} \int \frac{d^3k}{(2\pi)^3} (\omega - H(\mathbf{k}) - \Sigma + i0^+)^{-1}. \quad (6)$$

Eq. (6) can further be written as[16]

$$\Sigma = \Sigma_0 \mathbb{I}_2 + \Sigma_z \sigma_z, \quad (7)$$

where \mathbb{I}_2 is a 2×2 identity matrix, $\Sigma_0 = (\Sigma_{11} + \Sigma_{22})/2$, $\Sigma_z = (\Sigma_{11} - \Sigma_{22})/2$. Since the self-energy is momentum independent for δ -function correlated disorder, it simply modifies the parameters of the system as $\tilde{h} = h + \text{Re}\Sigma_z$, $\tilde{E}_F = E_F + \text{Re}\Sigma_0$, where ‘Re’ refers to the real part (of the self-energy). Note that $\Sigma_x(y)$ vanishes due to symmetry.

To compute Σ_z , we set $\Sigma = 0$ on the right-hand side of Eq. (6). This leads to

$$\Sigma_z = \frac{W^2}{3} \int \frac{d^3k}{(2\pi)^3} \frac{d_z}{E_F^2 - |d(\mathbf{k})|^2}. \quad (8)$$

Setting $E_F = 0$, we solve for Σ_z numerically at the gapless point with $h = -4$. Interestingly, we find $\Sigma_z > 0$. Consequently, the gapless point $h = -4$ shifts to $h - \Sigma_z$, enhancing the topological phase boundary as shown in Fig. (5).

IV. CONCLUSION AND OUTLOOK

We have studied the stability of the bulk gapped and boundary gapless states in a 3D CHI. Since there is no time-reversal or charge-conjugation symmetry, it is not obvious whether the topology of the system is protected against disorder. Interestingly, similar to conventional topological insulators, the disorder can drive a topological transition, and the gapless boundary states remain stable up to moderate disorder values. Investigating

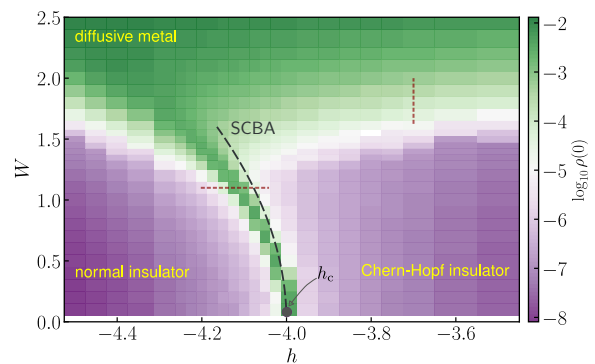


FIG. 5. Location of insulating regions, as diagnosed by the bulk density of states at zero energy. The observed finite width between two insulating phases arises from the limited resolution in the density of states calculation within the KPM method ($N_m=4097$ moments and 8 random vectors are used), with h_c marking the gap closing in the clean model (1). The dashed horizontal and vertical lines highlight the analysis points for finite-size scaling performed in Figs. 3, 4. The black dashed line shows the SCBA calculation of the phase boundary.

the Hopf-metal phase transition’s critical properties reveals a correlation length exponent of $\nu \simeq 1.0(1)$, deviating from traditional 3D delocalization-localization transitions across Wigner-Dyson universality classes (orthogonal $\nu \approx 1.571$ [82, 83], unitary $\nu \approx 1.43$ [84], symplectic $\nu \approx 1.375$ [85]), rather revealing the underlying Chern universality of the clean topological transition [86]. In comparison, a recent study in 3D orthogonal class with particle-hole symmetry undergoing topological to metallic transitions shows deviation from the standard universality class $\nu \approx 0.8$ [87].

In a situation where the transition is between semimetal and metal, such as the Weyl semimetal to diffusive metal, the correlation length exponent is found to be $\nu \approx 1.0$ [76, 78, 88]. The dynamical exponent at that transition was $z \approx 3/2$ due to the linear density of states $\rho(\varepsilon) \sim |\varepsilon|$ at the transition. In contrast, approaching the critical point from the metallic phase, we probe the dynamical exponent when $\rho(\varepsilon) \sim \varepsilon^2$ and finite at small energies, where one expects it to be $z \approx 1.0$; however, within our numerical accuracy we observe the slightly smaller value of $z \approx 0.85$.

We finally turned to Hopf insulators with zero Chern numbers. The phase diagram for these systems (data not shown here) is expected to be similar to that of the Hopf-Chern insulator. While we expect the critical properties to be identical, a detailed investigation is beyond the scope of this work due to computational limitations stemming from the long-range hopping inherent in the pure Hopf model. Moreover, identifying topological invariants in disordered Hopf-Chern insulators remains a challenge.

In closing, we explore possible experimental avenues for realizing such models and their associated physics.

Magnetic materials are highlighted as promising candidates for Hopf insulators, although specific materials fitting this description have yet to be identified. Layered Chern insulators with a twist [67] present promising options for Hopf insulators with non-zero Chern numbers. Consequently, helical magnets are considered optimal for realizing Hopf-Chern insulators and exploring disorder effects within these systems.

V. ACKNOWLEDGEMENTS

We would like to thank Bitan Roy and Robert-Jan Slager for a critical reading of the manuscript and for several insightful discussions. SB acknowledges support from MPG for funding through the Max Planck Partner Group at IIT Bombay. SB and KS thank the MPI-PKS, Dresden computing cluster, and the visitor program for their hospitality during the project. This work was partly supported by the Deutsche Forschungsgemeinschaft under the grant cluster of excellence ct.qmat (EXC 2147, project-id 390858490). KS also acknowledges funding from the Science and Engineering Research Board (SERB) under SERB-MATRICES Grant No. MTR/2023/000743 and support from the Department of Atomic Energy (DAE), Govt. of India, through the Basic Research in Physical and Multidisciplinary Sciences project via RIN4001.

Appendix A: Local charge impurities

In this section, we probe the stability of the transition and the associated critical properties by changing the nature of the disorder potential. Here we take the following onsite disorder potential $H_{\text{dis}} = \sum_{\mathbf{r}} |\mathbf{r}\rangle U(\mathbf{r}) \sigma_0 \langle \mathbf{r}|$. $U(\mathbf{r})$ is the strength of the potential, which is distributed over the interval $[-W, W]$.

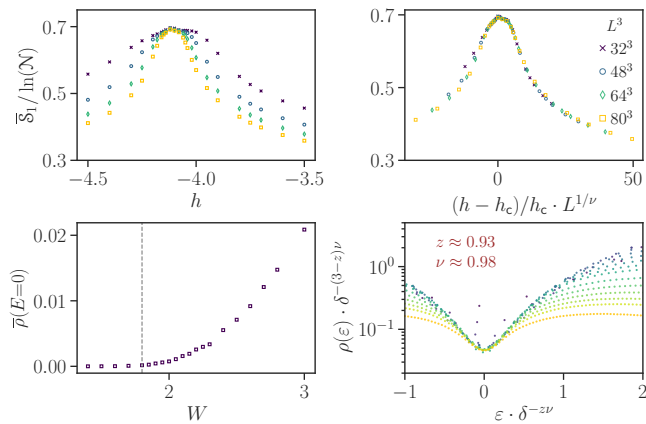


FIG. 6. Scaling collapse for the participation entropy \bar{S}_1 and also the density of states $\rho(E)$. The data supports $\nu \approx 1$, and the dynamical exponent $z \approx 0.93$.

The upper panel of Fig. 6 shows the scaling of $\bar{S}_1/\ln(N)$ as h is varied for different system sizes of linear length $L = 32 - 80$. The data clearly shows the transition between two different insulating phases at $h_c \simeq -4.115$, and the corresponding scaling collapse is shown with $\nu \approx 1$.

The lower panel shows the $E = 0$ density of states $\bar{\rho}$ calculated using the KPM method described in the main text. ρ becomes finite with increasing disorder, signifying the transition to the metallic phase. The scaling collapse of the metallic side's finite energy ρ supports critical exponents $z \approx 0.93$ and $\nu \approx 1$, which agrees with the staggered disorder data shown in the main text.

Appendix B: Fate of the surface state in the (100)-direction in the presence of disorder

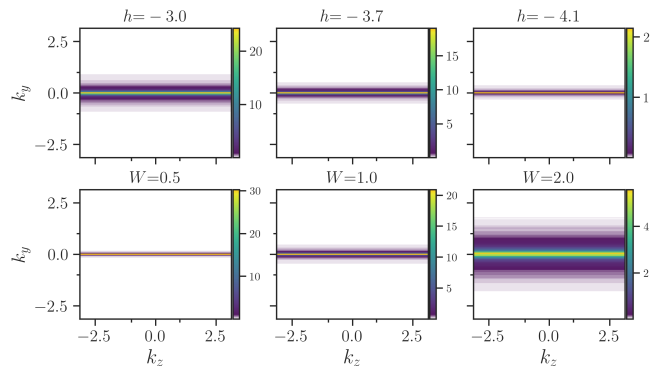


FIG. 7. Evolution of the surface spectral function at $E=0$ along the (100)-direction. All the parameters are the same as in Fig. 2. System size $\{Lx, Ly, Lz\} = \{64, 128, 128\}$.

Figure 7 shows the evolution of the surface spectral function $\mathcal{A}(k_y, k_z, E=0)$ (4) along the (100)-direction, with similar features observed in the (001) direction. At finite disorder $W = 1.1$ (upper panel of Fig. 7), transitioning from the topologically non-trivial phase to the trivial phase results in a significant reduction in the surface spectral weight, indicating the absence of the state in the trivial phase. Additionally, changing the disorder W at fixed $h = -3.7$, we observe the disappearance of the surface state as the system transitions into the diffusive metal phase, as mentioned in the main text.

Appendix C: Effective Surface Hamiltonian

In this section, we derive the effective Hamiltonian for the surface state along (001) direction. We terminate the lattice in the \hat{z} -direction, confining it within $z = 1$ and $z = L$, where L is the lattice length. Then, the momentum space Hamiltonian for the Chern-Hopf insulator

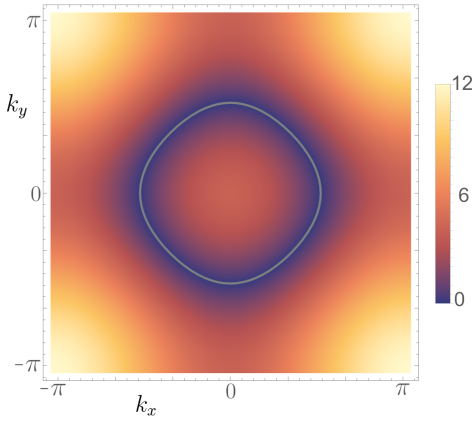


FIG. 8. The contour plot illustrates the energy difference $\Delta E = E_c - E_v$ between the two middle bands of the original surface state Hamiltonian, revealing a gapless nodal ring where $\Delta E = 0$. This alignment precisely coincides with the emergence of the gapless ring originating from d_z , as depicted by the white line.

discussed in the main text can be expressed as

$$\mathcal{H}(k_x, k_y) = \sum_{k_x, k_y, z=1}^{z=L} M_0(k_x, k_y) c_{k_x, k_y, z}^\dagger c_{k_x, k_y, z} + \mathcal{T}(k_x, k_y) c_{k_x, k_y, z}^\dagger c_{k_x, k_y, z+1} + h.c. \quad (\text{C1})$$

where $M_0(k_x, k_y) = (h + 2t(\cos(k_x) + \cos(k_y)))\sigma_z$ and $\mathcal{T}(k_x, k_y) = (-it_2 \sin(k_x) + t_2 \sin(k_y))\sigma_x + (it_2 \sin(k_y) + t_2 \sin(k_x))\sigma_y$.

To find the effective surface states, we choose the ansatz $\psi(z) = \lambda^z \phi$ to describe the localized, gapless surface states at the boundary. With this, the boundary equation becomes

$$d_z \sigma_z \phi + \lambda^{-1} t_2 (\sin k_y + i \sin k_x) \sigma_x \phi + \lambda^{-1} t_2 (\sin k_x - i \sin k_y) \sigma_y \phi = E \phi. \quad (\text{C2})$$

Solving this equation, we obtain $E = \pm d_z$, suggesting that the effective surface state Hamiltonian is $H_{\text{eff}} = d_z \sigma_z$. Fig. (8) demonstrates an exact correspondence between the effective surface state (depicted as a white ring) and the surface state found numerically by solving Eq. (C1). It turns out that for the other two directions, the effective surface state Hamiltonians are harder to find analytically. Thus, we only show the numerical solutions of the surface states in Fig. 1.

-
- [1] F. Evers and A. D. Mirlin, Anderson transitions, *Rev. Mod. Phys.* **80**, 1355 (2008).
- [2] Y. Asada, K. Slevin, and T. Ohtsuki, Anderson transition in two-dimensional systems with spin-orbit coupling, *Phys. Rev. Lett.* **89**, 256601 (2002).
- [3] M. Onoda, Y. Avishai, and N. Nagaosa, Localization in a quantum spin hall system, *Phys. Rev. Lett.* **98**, 076802 (2007).
- [4] A. D. Mirlin, F. Evers, I. V. Gornyi, and P. M. Ostrovsky, Anderson transitions: Criticality, symmetries and topologies, *International Journal of Modern Physics B* **24**, 1577 (2010), <https://doi.org/10.1142/S0217979210064526>.
- [5] S. Ryu, A. P. Schnyder, A. Furusaki, and A. W. W. Ludwig, Topological insulators and superconductors: tenfold way and dimensional hierarchy, *New Journal of Physics* **12**, 065010 (2010).
- [6] P. Goswami and S. Chakravarty, Quantum criticality between topological and band insulators in 3+1 dimensions, *Phys. Rev. Lett.* **107**, 196803 (2011).
- [7] L. Fu and C. L. Kane, Topology, delocalization via average symmetry and the symplectic anderson transition, *Phys. Rev. Lett.* **109**, 246605 (2012).
- [8] B. Roy, Y. Alavirad, and J. D. Sau, Global phase diagram of a three-dimensional dirty topological superconductor, *Phys. Rev. Lett.* **118**, 227002 (2017).
- [9] E. Prodan, Disordered topological insulators: a non-commutative geometry perspective, *Journal of Physics A: Mathematical and Theoretical* **44**, 113001 (2011).
- [10] M. Onoda, Y. Avishai, and N. Nagaosa, Localization in a quantum spin hall system, *Phys. Rev. Lett.* **98**, 076802 (2007).
- [11] K. Nomura, M. Koshino, and S. Ryu, Topological delocalization of two-dimensional massless dirac fermions, *Phys. Rev. Lett.* **99**, 146806 (2007).
- [12] H.-T. He, G. Wang, T. Zhang, I.-K. Sou, G. K. L. Wong, J.-N. Wang, H.-Z. Lu, S.-Q. Shen, and F.-C. Zhang, Impurity effect on weak antilocalization in the topological insulator Bi_2Te_3 , *Phys. Rev. Lett.* **106**, 166805 (2011).
- [13] H.-Z. Lu, J. Shi, and S.-Q. Shen, Competition between weak localization and antilocalization in topological surface states, *Phys. Rev. Lett.* **107**, 076801 (2011).
- [14] G. Schubert, H. Fehske, L. Fritz, and M. Vojta, Fate of topological-insulator surface states under strong disorder, *Phys. Rev. B* **85**, 201105 (2012).
- [15] H.-M. Guo, G. Rosenberg, G. Refael, and M. Franz, Topological anderson insulator in three dimensions, *Phys. Rev. Lett.* **105**, 216601 (2010).
- [16] C. W. Groth, M. Wimmer, A. R. Akhmerov, J. Tworzydło, and C. W. J. Beenakker, Theory of the topological anderson insulator, *Phys. Rev. Lett.* **103**, 196805 (2009).
- [17] J. Li, R.-L. Chu, J. K. Jain, and S.-Q. Shen, Topological anderson insulator, *Phys. Rev. Lett.* **102**, 136806 (2009).
- [18] E. Prodan, Disordered topological insulators: a non-commutative geometry perspective, *Journal of Physics*

- A: *Mathematical and Theoretical* **44**, 113001 (2011).
- [19] A. Yamakage, K. Nomura, K.-I. Imura, and Y. Kuramoto, Disorder-induced multiple transition involving z_2 topological insulator, *Journal of the Physical Society of Japan* **80**, 053703 (2011), <https://doi.org/10.1143/JPSJ.80.053703>.
- [20] E. Prodan, Three-dimensional phase diagram of disordered hgte/cdte quantum spin-hall wells, *Phys. Rev. B* **83**, 195119 (2011).
- [21] Y. Xing, L. Zhang, and J. Wang, Topological anderson insulator phenomena, *Phys. Rev. B* **84**, 035110 (2011).
- [22] B. Leung and E. Prodan, Effect of strong disorder in a three-dimensional topological insulator: Phase diagram and maps of the F_2 invariant, *Phys. Rev. B* **85**, 205136 (2012).
- [23] J. Song and E. Prodan, Aiii and bdi topological systems at strong disorder, *Phys. Rev. B* **89**, 224203 (2014).
- [24] P. V. Sriluckshmy, K. Saha, and R. Moessner, Interplay between topology and disorder in a two-dimensional semi-dirac material, *Phys. Rev. B* **97**, 024204 (2018).
- [25] Y.-B. Yang, K. Li, L.-M. Duan, and Y. Xu, Higher-order topological anderson insulators, *Phys. Rev. B* **103**, 085408 (2021).
- [26] Y.-S. Hu, Y.-R. Ding, J. Zhang, Z.-Q. Zhang, and C.-Z. Chen, Disorder and phase diagrams of higher-order topological insulators, *Phys. Rev. B* **104**, 094201 (2021).
- [27] S. Ryu and K. Nomura, Disorder-induced quantum phase transitions in three-dimensional topological insulators and superconductors, *Phys. Rev. B* **85**, 155138 (2012).
- [28] J. Song, H. Liu, H. Jiang, Q.-f. Sun, and X. C. Xie, Dependence of topological anderson insulator on the type of disorder, *Phys. Rev. B* **85**, 195125 (2012).
- [29] D. Xu, J. Qi, J. Liu, V. Sacksteder, X. C. Xie, and H. Jiang, Phase structure of the topological anderson insulator, *Phys. Rev. B* **85**, 195140 (2012).
- [30] A. Altland and M. R. Zirnbauer, Nonstandard symmetry classes in mesoscopic normal-superconducting hybrid structures, *Phys. Rev. B* **55**, 1142 (1997).
- [31] R. S. K. Mong, A. M. Essin, and J. E. Moore, Antiferromagnetic topological insulators, *Phys. Rev. B* **81**, 245209 (2010).
- [32] T. L. Hughes, E. Prodan, and B. A. Bernevig, Inversion-symmetric topological insulators, *Phys. Rev. B* **83**, 245132 (2011).
- [33] L. Fu, Topological crystalline insulators, *Phys. Rev. Lett.* **106**, 106802 (2011).
- [34] R.-J. Slager, A. Mesaros, V. Juričić, and J. Zaanen, The space group classification of topological band-insulators, *Nature Physics* **9**, 98 (2013).
- [35] C.-X. Liu, R.-X. Zhang, and B. K. VanLeeuwen, Topological nonsymmorphic crystalline insulators, *Phys. Rev. B* **90**, 085304 (2014).
- [36] C. Fang and L. Fu, New classes of three-dimensional topological crystalline insulators: Nonsymmorphic and magnetic, *Phys. Rev. B* **91**, 161105 (2015).
- [37] J. Kruthoff, J. de Boer, J. van Wezel, C. L. Kane, and R.-J. Slager, Topological classification of crystalline insulators through band structure combinatorics, *Phys. Rev. X* **7**, 041069 (2017).
- [38] Y. Xu, Z. Song, Z. Wang, H. Weng, and X. Dai, Higher-order topology of the axion insulator euin_2as_2 , *Phys. Rev. Lett.* **122**, 256402 (2019).
- [39] Z.-D. Song, B. Lian, R. Queiroz, R. Ilan, B. A. Bernevig, and A. Stern, Delocalization transition of a disordered axion insulator, *Phys. Rev. Lett.* **127**, 016602 (2021).
- [40] H. Li, H. Jiang, C.-Z. Chen, and X. C. Xie, Critical behavior and universal signature of an axion insulator state, *Phys. Rev. Lett.* **126**, 156601 (2021).
- [41] W. A. Benalcazar, B. A. Bernevig, and T. L. Hughes, Quantized electric multipole insulators, *Science* **357**, 61 (2017).
- [42] W. A. Benalcazar, B. A. Bernevig, and T. L. Hughes, Electric multipole moments, topological multipole moment pumping, and chiral hinge states in crystalline insulators, *Phys. Rev. B* **96**, 245115 (2017).
- [43] F. Schindler, A. M. Cook, M. G. Vergniory, Z. Wang, S. S. P. Parkin, B. A. Bernevig, and T. Neupert, Higher-order topological insulators, *Science Advances* **4**, eaat0346 (2018).
- [44] M. Ezawa, Higher-order topological insulators and semimetals on the breathing kagome and pyrochlore lattices, *Phys. Rev. Lett.* **120**, 026801 (2018).
- [45] H. Araki, T. Mizoguchi, and Y. Hatsugai, Phase diagram of a disordered higher-order topological insulator: A machine learning study, *Phys. Rev. B* **99**, 085406 (2019).
- [46] C. Wang and X. R. Wang, Disorder-induced quantum phase transitions in three-dimensional second-order topological insulators, *Phys. Rev. Res.* **2**, 033521 (2020).
- [47] C.-A. Li, B. Fu, Z.-A. Hu, J. Li, and S.-Q. Shen, Topological phase transitions in disordered electric quadrupole insulators, *Phys. Rev. Lett.* **125**, 166801 (2020).
- [48] A. Agarwala, V. Juričić, and B. Roy, Higher-order topological insulators in amorphous solids, *Phys. Rev. Res.* **2**, 012067 (2020).
- [49] A. L. Szabó and B. Roy, Dirty higher-order dirac semimetal: Quantum criticality and bulk-boundary correspondence, *Phys. Rev. Res.* **2**, 043197 (2020).
- [50] P. Zhu, T. L. Hughes, and A. Alexandradinata, Quantized surface magnetism and higher-order topology: Application to the hopf insulator, *Phys. Rev. B* **103**, 014417 (2021).
- [51] J. E. Moore, Y. Ran, and X.-G. Wen, Topological surface states in three-dimensional magnetic insulators, *Phys. Rev. Lett.* **101**, 186805 (2008).
- [52] D.-L. Deng, S.-T. Wang, C. Shen, and L.-M. Duan, Hopf insulators and their topologically protected surface states, *Phys. Rev. B* **88**, 201105(R) (2013).
- [53] Z. Yan, R. Bi, and Z. Wang, Majorana zero modes protected by a hopf invariant in topologically trivial superconductors, *Phys. Rev. Lett.* **118**, 147003 (2017).
- [54] C. Liu, F. Vafa, and C. Xu, Symmetry-protected topological hopf insulator and its generalizations, *Phys. Rev. B* **95**, 161116(R) (2017).
- [55] A. Alexandradinata, A. Nelson, and A. A. Soluyanov, Teleportation of berry curvature on the surface of a hopf insulator, *Phys. Rev. B* **103**, 045107 (2021).
- [56] P. Zhu, T. L. Hughes, and A. Alexandradinata, Quantized surface magnetism and higher-order topology: Application to the hopf insulator, *Phys. Rev. B* **103**, 014417 (2021).
- [57] Y.-G. Yue and Z.-X. Liu, Realization of the topological hopf term in two-dimensional lattice models, *Phys. Rev. B* **107**, 045130 (2023).
- [58] B. Lapierre, T. Neupert, and L. Trifunovic, n -band hopf insulator, *Phys. Rev. Res.* **3**, 033045 (2021).
- [59] A. Nelson, T. Neupert, A. Alexandradinata, and T. c. v. Bzdušek, Delicate topology protected by rotation symmetry: Crystalline hopf insulators and beyond, *Phys. Rev.*

- B **106**, 075124 (2022).
- [60] P. G. Yuxin Wang, Alexander C. Tyner, Fundamentals of crystalline hopf insulators (2023), arXiv:2301.08244 [cond-mat.mes-hall].
- [61] W. J. Jankowski, A. S. Morris, Z. Davoyan, A. Bouhon, F. N. Ünal, and R.-J. Slager, Non-abelian hopf-euler insulators (2024), arXiv:2405.17305 [cond-mat.mes-hall].
- [62] R. S. K. Mong, A. M. Essin, and J. E. Moore, Antiferromagnetic topological insulators, *Phys. Rev. B* **81**, 245209 (2010).
- [63] A. Bouhon, T. c. v. Bzdušek, and R.-J. Slager, Geometric approach to fragile topology beyond symmetry indicators, *Phys. Rev. B* **102**, 115135 (2020).
- [64] F. N. Ünal, A. Bouhon, and R.-J. Slager, Topological euler class as a dynamical observable in optical lattices, *Phys. Rev. Lett.* **125**, 053601 (2020).
- [65] F. N. Ünal, A. Eckardt, and R.-J. Slager, Hopf characterization of two-dimensional floquet topological insulators, *Phys. Rev. Res.* **1**, 022003(R) (2019).
- [66] B. P. Parasar and V. B. Shenoy, Delicate semimetals: Protected gapless phases from unstable homotopies, *Phys. Rev. B* **109**, 155131 (2024).
- [67] R. Kennedy, Topological hopf-chern insulators and the hopf superconductor, *Phys. Rev. B* **94**, 035137 (2016).
- [68] I. Dutta and K. Saha, Flat bands in three-dimensional lattice models with non-trivial hopf index, *New Journal of Physics* **26**, 073051 (2024).
- [69] R.-J. Slager, V. Juričić, and B. Roy, Dissolution of topological fermi arcs in a dirty weyl semimetal, *Phys. Rev. B* **96**, 201401 (2017).
- [70] K. Slevin and T. Ohtsuki, Corrections to scaling at the anderson transition, *Phys. Rev. Lett.* **82**, 382 (1999).
- [71] X. Jia, A. R. Subramaniam, I. A. Gruzberg, and S. Chakravarty, Entanglement entropy and multifractality at localization transitions, *Phys. Rev. B* **77**, 014208 (2008).
- [72] C. W. Groth, M. Wimmer, A. R. Akhmerov, and X. Waintal, Kwant: a software package for quantum transport, *New Journal of Physics* **16**, 063065 (2014).
- [73] E. Abrahams, P. W. Anderson, D. C. Licciardello, and T. V. Ramakrishnan, Scaling theory of localization: Absence of quantum diffusion in two dimensions, *Phys. Rev. Lett.* **42**, 673 (1979).
- [74] K. Slevin, P. Markoš, and T. Ohtsuki, Reconciling conductance fluctuations and the scaling theory of localization, *Phys. Rev. Lett.* **86**, 3594 (2001).
- [75] A. Weiße, G. Wellein, A. Alvermann, and H. Fehske, The kernel polynomial method, *Rev. Mod. Phys.* **78**, 275 (2006).
- [76] K. Kobayashi, T. Ohtsuki, K.-I. Imura, and I. F. Herbut, Density of states scaling at the semimetal to metal transition in three dimensional topological insulators, *Phys. Rev. Lett.* **112**, 016402 (2014).
- [77] S. Liu, T. Ohtsuki, and R. Shindou, Effect of disorder in a three-dimensional layered chern insulator, *Phys. Rev. Lett.* **116**, 066401 (2016).
- [78] S. Bera, J. D. Sau, and B. Roy, Dirty weyl semimetals: Stability, phase transition, and quantum criticality, *Phys. Rev. B* **93**, 201302 (2016).
- [79] J. H. Pixley, P. Goswami, and S. Das Sarma, Disorder-driven itinerant quantum criticality of three-dimensional massless dirac fermions, *Phys. Rev. B* **93**, 085103 (2016).
- [80] E. Prodan, T. L. Hughes, and B. A. Bernevig, Entanglement spectrum of a disordered topological chern insulator, *Phys. Rev. Lett.* **105**, 115501 (2010).
- [81] M. Moreno-Gonzalez, J. Dieplinger, and A. Altland, Topological quantum criticality of the disordered chern insulator, *Annals of Physics* **456**, 169258 (2023).
- [82] A. Rodriguez, L. J. Vasquez, K. Slevin, and R. A. Römer, Critical parameters from a generalized multifractal analysis at the anderson transition, *Phys. Rev. Lett.* **105**, 046403 (2010).
- [83] K. Slevin and T. Ohtsuki, Critical exponent for the anderson transition in the three-dimensional orthogonal universality class, *New Journal of Physics* **16**, 015012 (2014).
- [84] K. Slevin and T. Ohtsuki, The anderson transition: Time reversal symmetry and universality, *Phys. Rev. Lett.* **78**, 4083 (1997).
- [85] Y. Asada, K. Slevin, and T. Ohtsuki, Anderson transition in the three dimensional symplectic universality class, *Journal of the Physical Society of Japan* **74**, 238 (2005).
- [86] M. D. Caio, G. Möller, N. R. Cooper, and M. J. Bhaseen, Topological marker currents in chern insulators, *Nature Physics* **15**, 257 (2019).
- [87] X. Luo, B. Xu, T. Ohtsuki, and R. Shindou, Critical behavior of anderson transitions in three-dimensional orthogonal classes with particle-hole symmetries, *Phys. Rev. B* **101**, 020202 (2020).
- [88] B. Roy, R.-J. Slager, and V. Juričić, Global phase diagram of a dirty weyl liquid and emergent superuniversality, *Phys. Rev. X* **8**, 031076 (2018).